CHEMISTRY OF MATERIALS

pubs.acs.org/cm

Article

Hydroquinone-Based Synthesis of Pd Nanostructures and the Interplay of Surface Capping, Reduction Kinetics, Attachment, Diffusion, and Fusion

Anderson G. M. da Silva, Ruhui Chen, Quynh N. Nguyen, Madeline Vara, Pedro H. C. Camargo, and Younan Xia*

Cite This: *Chem. Mater.* 2021, 33, 8430–8439

Read Online

ACCESS | Metrics & More | Article Recommendations | Supporting Information

ABSTRACT: The rational synthesis of nanostructured materials with desired properties calls for a thorough understanding of the growth mechanism. Here we report a mechanistic case study of Pd nanostructures synthesized by reducing a Pd(II) precursor with hydroquinone in the presence of KBr. As the reaction temperature was decreased from 100 to 20 °C, sub-10 nm cubes, concave nanocubes, and cube-like aggregates of much smaller particles were sequentially obtained. Our time-lapse experiments and a set of controls indicated that primary particles of 1−4 nm in size were formed during the initial stage of the synthesis, followed by their aggregation into cube-like structures through an attachment process. In addition to the influence of surface capping, the reaction temperature played a vital role in determining the exact shape or morphology of the final products by affecting the reduction kinetics, fusion of the attached particles, and surface diffusion of atoms. At 100 °C, corresponding to a quick depletion of the Pd(II) precursor, the primary particles in each aggregate could easily fuse together to form nanocubes with flat faces owing to adequate surface diffusion. At 60 °C, the constituent particles also fused into cubes and then evolved into concave cubes through atomic deposition at the corners. At 20 °C, although fusion did not occur due to the substantially decreased diffusion rate, the primary particles in each aggregate still grew through atomic deposition for the formation of larger, cube-like aggregates. Explicating the growth mechanism, this work offers a mechanistic understanding of the nonclassical growth mode involved in the formation of various metal nanostructures.

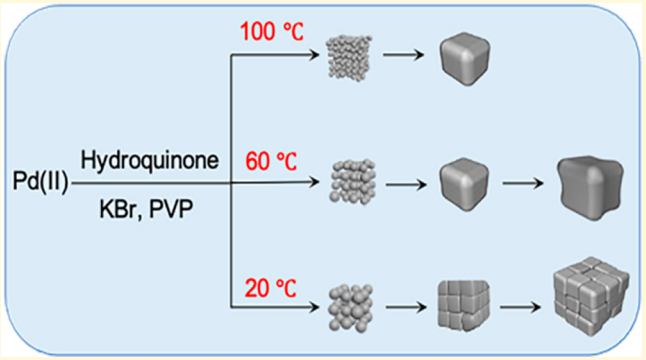

INTRODUCTION

Among the broad range of parameters that influence the properties and applications of metal nanostructures,[1−5] the shape or morphology has received extensive attention as precise control of this parameter provides a simple yet versatile strategy for tailoring the performance of a metal nanostructure in a specific application.[6−9] A compelling example can be found in the synthesis of Pd nanocubes with a well-defined surface structure. The Pd nanocubes encased by {100} facets are significantly more active toward the formic acid oxidation than nanocrystals in other shapes, including the {111}-terminated octahedral and tetrahedral counterparts.[10] When the conventional nanocubes evolved into concave cubes under kinetically regulated growth, they exhibited further enhancement of catalytic activity due to the creation of high-index facets on the surface.[11] In both cases, the emergence of nanostructures with improved performance is subject to well-controlled nucleation and growth pathways, which can dictate the shape or morphology finally taken by the nanostructures.[12−14]

The growth mechanism of metal nanostructures has been studied and postulated ever since the first synthesis was reported. According to the classical theory described by the LaMer model, the metal precursor is first reduced to atoms, followed by their agglomeration to generate nuclei once the concentration of atoms surpasses the supersaturation level.[15] Afterward, the nuclei evolve into seeds with certain internal structures and grow into larger nanostructures with different shapes through atomic addition. Although it was built upon many oversimplified assumptions and was challenged in recent years, the classical theory remains an appropriate model for describing the important aspects of nucleation in a solution-based system and offers guidelines for synthesizing nanostruc-

Received: August 12, 2021
Revised: October 7, 2021
Published: October 22, 2021

https://doi.org/10.1021/acs.chemmater.1c02791
Chem. Mater. 2021, 33, 8430−8439

tures with a uniform size distribution. Because of recent advancements in characterization techniques, several secondary processes such as particle coalescence, Ostwald ripening, and oriented attachment have been proposed as alternative routes to account for the growth of metal nanostructures.[16−18] For example, both Pd worm-like nanowires[19] and Pt mesoporous nanocubes[20] were generated through attachment-based growth, and their unique morphologies led to outstanding performance in catalytic applications. Despite the appealing features enabled by nonclassical growth pathways, the ability to achieve specific shapes or morphologies is still limited due to the lack of incisive understanding of the mechanism governing the growth process. Collectively, a number of parameters, including the reduction kinetics, surface capping, adatom diffusion, particle attachment, and fusion, can affect the growth patterns and thus the shape or morphology taken by the final product. Although effort has been devoted to investigating these factors, the interplay among them remains elusive and needs further exploration. A comprehensive understanding of these underlying factors will allow us to move away from the traditional trial-and-error approach and produce metal nanostructures with desired shapes and properties in a more deterministic and robust fashion.

In this work, we report a mechanistic study of Pd nanostructures with various morphologies resulting from the nonclassical, attachment-based growth. The experiments involved a single-step synthesis, in which the Pd(II) precursor was reduced by hydroquinone in the presence of Br^- ions as a capping agent. When the reaction temperature was decreased from 100 to 20 °C, different types of Pd nanostructures, including sub-10 nm nanocubes, concave nanocubes, and cube-like aggregates assembled from small primary particles, could be sequentially obtained. Our probe of the growth mechanism revealed that cube-like aggregates were initially formed as intermediates through the attachment of Pd primary particles and the effect of surface capping. The reaction temperature was found to play a deterministic role in defining the exact shape or morphology of the final products by influencing the reduction kinetics, surface diffusion, and fusion of the attached particles. At a high temperature of 100 °C, the primary particles in each aggregate could fuse together to form nanocubes with flat faces owing to the capping effect of Br^- ions and adequate surface diffusion. On the contrary, moderate reduction and surface diffusion rates, both associated with an intermediate temperature of 60 °C, also induced the fusion of the attached particles into nanocubes, followed by atomic deposition at the corners for the generation of concave cubes. In contrast, the fusion process was inhibited at a low temperature of 20 °C, but the constituent particles in each aggregate still grew through atomic deposition and gradually evolved into larger, cube-like aggregates. The ability to rationally manipulate these kinetic parameters by varying the reaction temperature, in addition to the use of an appropriate capping agent, is the prerequisite for the successful synthesis of well-defined Pd nanostructures with the desired morphology through nonclassical growth.

EXPERIMENTAL SECTION

Chemicals and Materials. Potassium tetrachloropalladate trihydrate ($K_2PdCl_4·3H_2O$, 98%), poly(vinylpyrrolidone) (PVP; MW ≈ 55000), hydroquinone ($C_6H_6O_2$, 99%), and potassium bromide (KBr, 99%) were all obtained from Sigma-Aldrich and used as received. All solutions were prepared using deionized water with a resistivity of 18.2 MΩ cm at room temperature.

Synthesis of the Pd Nanostructures. For a standard synthesis, 10 mL of an aqueous solution containing 100 mg of PVP was added to a 20 mL round-bottom flask (immersed in an oil bath held at 60 °C) and stirred for 10 min, followed by the introduction of 100 μL of aqueous KBr (120 mM) and 1 mL of aqueous K_2PdCl_4 (12 mM). After 2 min, 1 mL of aqueous hydroquinone (30 mM) was added, and the reaction was allowed to proceed for 24 h. The solid products were then isolated by centrifugation at 55000 rpm for 30 min and washed three times with ethanol and another three times with water. Afterward, they were dispersed in 10 mL of water for further characterizations. A set of control experiments were also carried out at 20, 40, 50, 60, 80, and 100 °C by following the standard protocol. To elucidate the growth mechanism, the synthesis conducted at 20, 60, and 100 °C was quenched at different time points by cooling the reaction mixture with an ice/water bath.

Characterizations. Transmission electron microscopy (TEM) images were taken on a Hitachi HT7700 microscope operated at 120 kV. Secondary electron (SE), bright-field (BF), and high-angle annular dark-field (HAADF) scanning TEM (STEM) images were obtained using a Hitachi HD2700 microscope, with a STEM aberration corrector, operated at 200 kV. Samples for TEM analysis were prepared by drop-casting an aqueous suspension of the nanoparticles on a carbon-coated copper grid, followed by drying under ambient conditions. The concentrations of Pd(II) ions remaining in the reaction mixture at different time points during a synthesis were analyzed using an inductively coupled plasma mass spectrometer (ICP-MS, PerkinElmer, NexION 300Q).

RESULTS AND DISCUSSION

Evolution of the Pd Nanostructures at Different Reaction Temperatures. Our investigation started with the reduction of Pd(II) by hydroquinone at 100 °C in the presence of PVP as a colloidal stabilizer and Br^- ions from KBr as a capping agent toward Pd{100} facets. Five minutes into the synthesis, we obtained Pd nanocubes with an average edge length of 6 ± 2 nm, as shown in Figure S1. To further elucidate factors that determine the size and shape of the Pd nanostructures, we carried out a set of experiments at different temperatures. Figure 1 shows a summary of the products obtained at different temperatures, demonstrating their variations in both size and morphology as a function of reaction temperature. Specifically, as the reaction temperature decreased, the nanostructures gradually grew, from an average edge length of 6 ± 2 nm at 100 °C to 45 ± 4 nm at 20 °C. This observation is consistent with the general explanation that fewer seeds would be produced in the nucleation stage at a lower temperature due to the decelerated initial reduction rate. As a result, more precursors would be allocated to each seed during the growth process for the generation of larger nanostructures.[21] In addition to the increase in dimensions, the morphology of the products gradually evolved from cubes to concave cubes and finally cube-like aggregates as the reaction temperature decreased from 100 to 20 °C.

We then used STEM to characterize the Pd nanostructures obtained at three different temperatures of 100, 60, and 20 °C to further analyze their distinct morphologies. As shown in Figure 2A−C, the nanocrystal obtained at 100 °C exhibited a cubic shape with an edge length of ∼6 nm and evident single crystallinity. The well-resolved lattice fringes gave a spacing of ∼0.19 nm, corresponding to the {200} planes of face-centered cubic (*fcc*) Pd. Interestingly, decreasing the temperature from 100 to 60 °C led to the generation of larger and noticeably concave nanocubes with an edge length of ∼15 nm (Figure 2D−F and Figure S2). In addition to the lattice fringes

https://doi.org/10.1021/acs.chemmater.1c02791
Chem. Mater. 2021, 33, 8430−8439

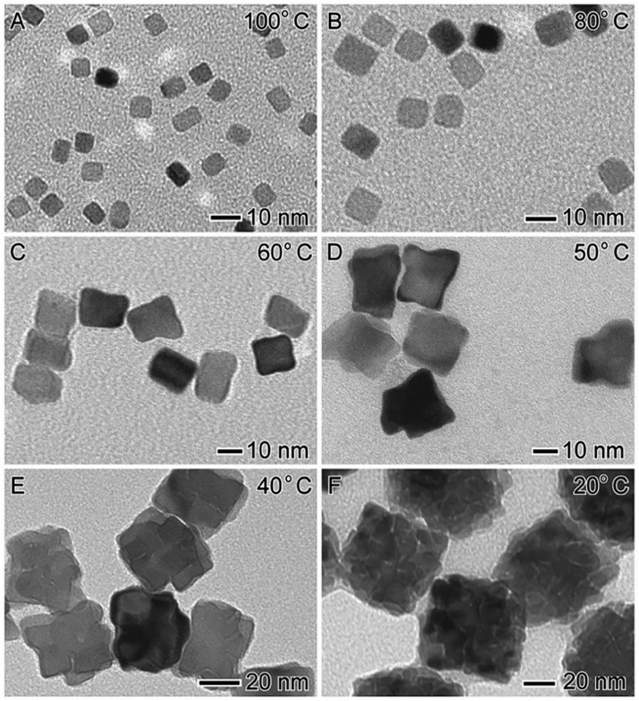

Figure 1. TEM images of the Pd nanostructures obtained by reducing a Pd(II) precursor with hydroquinone in an aqueous system for 24 h in the presence of KBr at (A) 100, (B) 80, (C) 60, (D) 50, (E) 40, and (F) 20 °C. The nanostructures grew and gradually transformed from cubes to concave cubes and cube-like aggregates as the reaction temperature was decreased.

corresponding to Pd{100} planes, we clearly observed the protuberance at the corners of the cubes and thus the inward curvature of the side faces. When the reaction temperature was further decreased to 20 °C, large pseudocubic aggregates with an edge length of ~45 ± 4 nm were produced, which consisted of multiple primary particles of 6−7 nm in size (Figure 2G,H and Figure S3). The continuous lattice fringes observed in Figure 2I could also be indexed to Pd{200}, revealing that the primary particles of the cube-like aggregates were monocrystalline.

In an effort to elucidate the mechanistic details, we collected and analyzed the intermediates involved in the evolution of the Pd nanostructures by quenching the synthesis at different time points. Figure 3 shows the results from a synthesis conducted

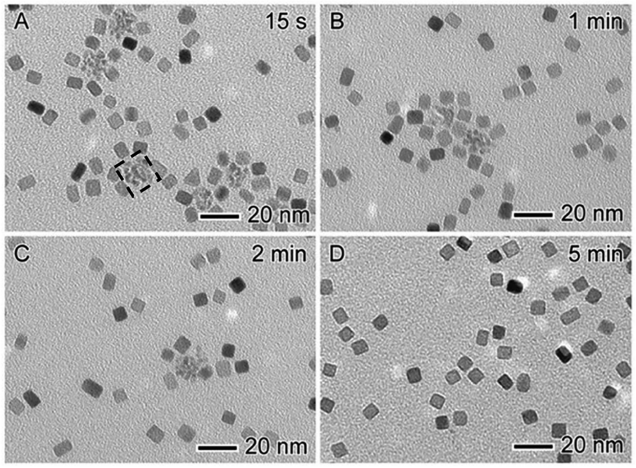

Figure 3. TEM images of the Pd nanostructures obtained at different stages of a standard synthesis conducted at 100 °C: (A) 15 s, (B) 1 min, (C) 2 min, and (D) 5 min. Only 15 s into the synthesis, the sample was already dominated by Pd nanocubes with an edge length of ~6 nm. As indicated by the box in panel A, the nanocubes were likely formed through an attachment mechanism, followed by fusion of the constituent particles and then recrystallization as a result of adequate surface diffusion and the capping effect of Br^- ions toward Pd{100} facets. At 5 min into the synthesis, the products contained only nanocubes.

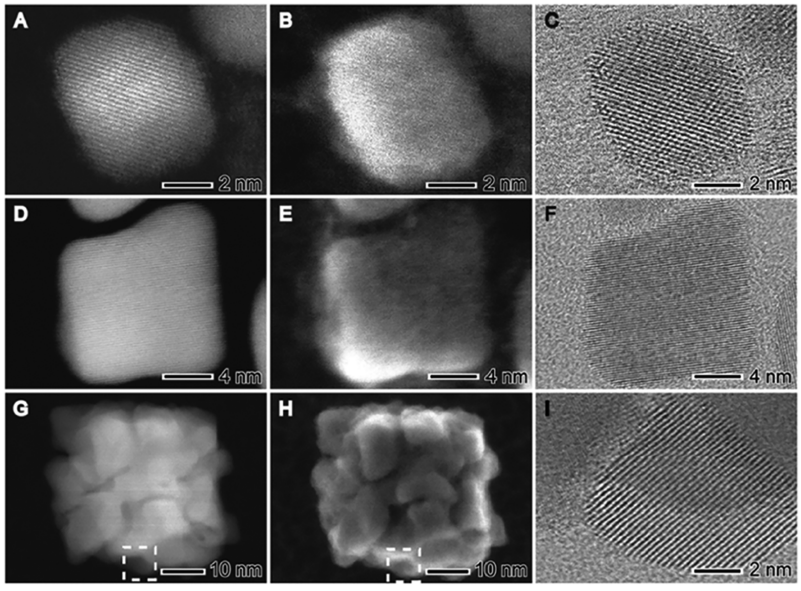

Figure 2. Typical HAADF-, SE-, and BF-STEM images (from left to right in each row, respectively) of the Pd nanostructures obtained using the standard protocol except for the difference in reaction temperature: (A−heC) 100 °C, (D−F) 60 °C, and (G−I) 20 °C. The region marked by dashed squares in panels G and H is detailed in panel I. The lattice fringes observed in all of the BF-STEM images corresponded to Pd{200} planes.

https://doi.org/10.1021/acs.chemmater.1c02791
Chem. Mater. 2021, 33, 8430−8439

at 100 °C. Only 15 s after the introduction of hydroquinone, a large number of ∼5 nm Pd cubes were already produced, together with some loose, cube-like aggregates comprised of primary particles of 1−2 nm in size (Figure 3A). At 1 and 2 min into the synthesis (Figure 3B,C), the aggregates significantly decreased in number, suggesting that the nanocubes were likely derived from the aggregates through fusion, as confirmed by the major decrease in volume. At 5 min (Figure 3D), all of the aggregates disappeared, and the final products contained only cubes with an edge length of ∼6 nm. The formation of flat faces on the nanocubes could be ascribed to the adequate diffusion of surface atoms at 100 °C, coupled with the selective binding of Br^- ions to the {100} facets. Afterward, no further change in the size or shape was observed up to 24 h into the synthesis (Figure 1A). On the basis of these results, we argue that the formation of the Pd nanocubes was initiated by the attachment of primary particles (1−2 nm in size), followed by their fusion and then recrystallization, as a result of adequate surface diffusion at the increased temperature and the capping of Pd{100} facets by Br^- ions.

When the synthesis was conducted at a lower temperature of 60 °C, a similar growth pattern was observed, except that the preformed nanocubes eventually evolved into concave cubes as a result of site-selective atomic deposition in the late stage of the synthesis. Figure 4 shows a series of TEM images to illustrate the morphological evolution of the nanocrystals during the prolonged reaction time. Similar to the observations at 100 °C, both nearly cubic nanocrystals and loose, cube-like aggregates of primary particles (2−3 nm in size) were present in the early stage of the synthesis (Figure 4A). When characterized by STEM, the cube-like aggregates were polycrystalline while the nanocubes showed a single-crystal structure (Figure S4), further attesting to the hypothesis that the nanocubes were derived from aggregates of smaller primary particles through attachment, fusion, and recrystallization. At 1 min into the synthesis, almost 50% of the aggregates had evolved into nanocrystals with a cubic shape (Figure 4B). This stage also marked the beginning of the site-selected atomic deposition, where the as-obtained nanostructures adopted a pseudocubic morphology, with both smooth {100} facets and corner rounding visible on some particles, in addition to a small degree of asymmetry. As the reaction proceeded to 2, 5, and 10 min, the nanocubes gradually evolved into concave cubes with increased sizes and noticeable protuberance at the corners (Figure 4C−E), which possibly arose from the selective deposition of the newly formed Pd atoms on corner sites of the nanocubes. The generation of concave nanocubes could be ascribed to the capping effect, as well as moderate surface diffusion and fusion rates typical of an intermediate temperature. These factors directed the newly formed Pd atoms to pile up at the corners and edges of the preformed nanocubes where the surface energy is higher than those of other sites, instead of quickly diffusing to {100} faces for the generation of regular cubes. When the reaction proceeded to 1 h, all of the primary particles disappeared, leaving behind concave nanocubes as the main product (Figure 4F).

A similar trend was also observed at the beginning of a synthesis conducted at a significantly lower temperature, except that the growth pathway determining the morphology of final products was different. Figure 5 shows the products obtained at different stages of the synthesis conducted at 20 °C. After 2 h into the synthesis, we observed single-crystal particles with an average size of 2−4 nm (Figure 5A). Extension of the reaction time to 3 h led to the formation of cube-like aggregates (Figure 5B), similar to the outcomes observed in the syntheses carried out at 60 and 100 °C, albeit

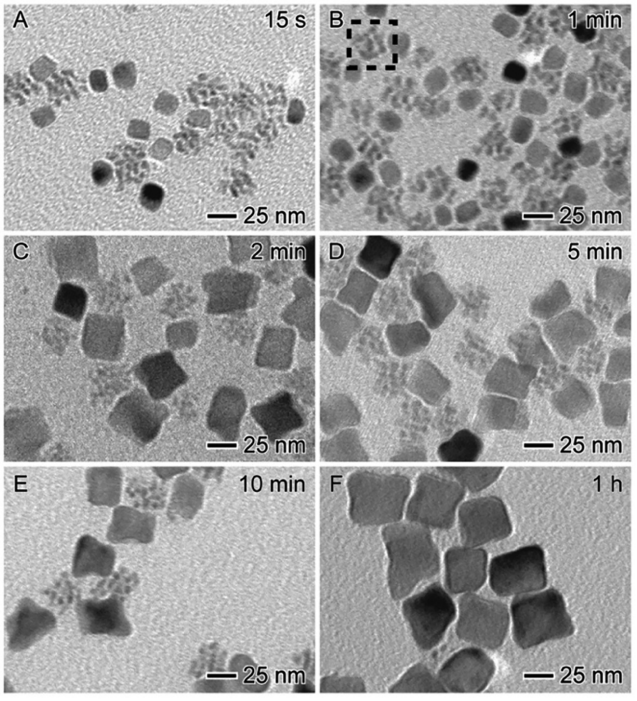

Figure 4. TEM images of the Pd nanostructures obtained at different time points of a standard synthesis conducted at 60 °C: (A) 15 s, (B) 1 min, (C) 2 min, (D) 5 min, (E) 10 min, and (F) 1 h. At 1 min into the synthesis, almost 50% of the aggregates, as indicated by the box in panel B, had evolved into nanocubes as a result of fusion, recrystallization, and faceting. Afterward, the nanocubes could serve as seeds for the atomic deposition at corners and edges, gradually evolving into concave cubes.

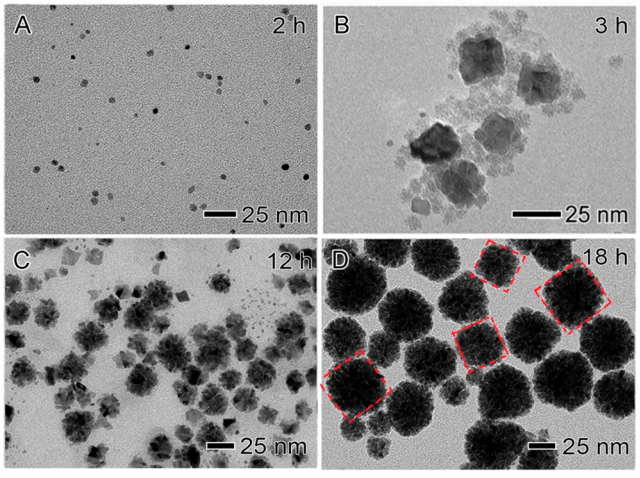

Figure 5. TEM images of the Pd nanostructures obtained at different time points in a standard synthesis conducted at 20 °C: (A) 2 h, (B) 3 h, (C) 12 h, and (D) 18 h. The red dashed line in panel D outlines the pseudocubic profile of the aggregates. Primary particles of 2−4 nm in size were produced in the initial stage, followed by their attachment to form cube-like aggregates and then densification of the aggregates through atomic deposition.

https://doi.org/10.1021/acs.chemmater.1c02791
Chem. Mater. 2021, 33, 8430−8439

after a much longer period of time. As the synthesis was continued for 12 and 8 h, the preformed aggregates grew much larger in size but still maintained a partially cubic morphology (Figure 5C,D). As the reaction approached an equilibrium state at 24 h, these aggregates transformed into a more cubic shape with no significant change in size (Figure 1F). We could also observe some particles attached to the surface of the aggregates obtained at 3 and 12 h (Figure 5B,C), suggesting that the overgrowth of primary particles in each aggregate induced the generation of larger, cube-like aggregates. We proposed that the substantially slow reduction and adatom diffusion rates at 20 °C resulted in the initial formation of primary particles, followed by their growth via attachment to evolve into small aggregates as intermediates and then larger, cube-like aggregates through atomic deposition, even though the fusion process did not occur to promote the production of cubic nanocrystals. Table S1 shows a summary of the size and morphology of the primary particles and final products, as well as proposed growth pathways when the synthesis was conducted at three different temperatures.

Role of Surface Capping. In addition to the reaction temperature, we also investigated the role played by Br^- ions in the formation of cubic nanostructures. A set of experiments was performed under the same conditions as in the standard protocol, except for variation of the amount of KBr added to the reaction mixture. Figure S5 shows the evolution of morphology in a synthesis conducted at 60 °C in the absence of KBr. Although small aggregates comprised of primary particles were produced only after 5 and 15 s into the reaction, they did not evolve into a cubic shape in the absence of KBr (Figure S5A,B). Consequently, as the reaction proceeded to 1 min, larger aggregates with pseudospherical instead of cubic shape were generated, possibly through the growth of the constituent particle, demonstrating the critical role played by Br^- ions in shape control (Figure S5C). These nearly spherical aggregates then served as seeds for additional atomic deposition, leading to the production of larger nanostructures (Figure S5D). The size of these larger aggregates assembled from primary particles continued to increase until 30 min into the reaction when all remaining precursors in the reaction solution were depleted (Figure S5E,F). As suggested by the experimental results, Br^- ions not only directed the Pd aggregates to evolve into a cubic shape for the following fusion process but also posed a capping effect on the recrystallization of the particles to form {100} facets. No single-crystal, cubic nanostructures could be obtained in the absence of KBr.

Due to the preferential adsorption of Br^- ions onto the Pd{100} facets,[22] the introduction of KBr is expected to favor the formation of Pd nanostructures enclosed by {100} facets. However, variation in the amount of KBr introduced into the synthesis could also change the size and shape of the final products. Figure S6 shows TEM images of Pd nanostructures obtained when the syntheses were conducted at 60 °C with a sequential increase in the concentration of KBr. When only 20 μL of the 120 mM KBr solution was added, nearly spherical nanoparticles were formed, likely due to the insufficient capping effect from a low concentration of Br^- ions (Figure S6A). As the amount of Br^- ions was further increased, concave cubes were obtained as in the standard protocol (Figure S6B–D). On the contrary, when Br^- ions were in great excess, anisotropic growth took place, leading to the generation of elongated nanobars with a concave surface (Figure S6E,F). This outcome could be ascribed to the substantially enhanced oxidative etching from the highly concentrated Br^- ions, which selectively activated one side face of the nanocubes and resulted in the preferential atomic deposition and elongation along this direction.[23] These observations are in agreement with our results obtained at 100 °C, in which Pd nanocubes enclosed by {100} facets become evident with an increase in the amount of Br^- ions (Figure S7A–D). With a large amount of KBr, Pd nanobars enclosed by {100} facets were finally obtained (Figure S7E,F), in accord with previous reports about the formation of nanobars.[23,24]

The capping effect of Br^- ions could also be used to rationalize the postulation based on TEM images that attachment processes dominated in the synthesis of sub-10 nm Pd cubes at 100 °C reported herein, whereas atomic deposition prevailed as the primary growth pathway in the conventional protocol (Table S2). Because of their high surface energy and great mobility at increased temperatures, the small primary particles formed in the initial stage of a synthesis would prefer to collide with and attach to each other to reduce the total surface free energy. In addition to modulating the morphologies of building blocks, the capping agent adsorbed on the surface of those primary particles could act as a physical barrier to enhance the steric hindrance, thus impacting the interparticle interactions during their assembly.[25,26] Therefore, the coverage density and strength of the capping agent should be considered when evaluating the likelihood of particle attachment. Notably, the concentration of Br^- ions as a capping agent in the conventional protocol[27] was approximately 200 times higher than what was used in this work (Table S2). The extremely dense layer of Br^- ions on the surface, coupled with a relatively larger amount of PVP as a colloidal stabilizer, would elongate the distances between primary particles and thus hinder their aggregation in the conventional synthesis. As an alternative growth pathway, the newly produced atoms would continuously be deposited on the surface of the primary particles, followed by their diffusion across the surface for the generation of nanocubes as final products. In contrast, a substantially low concentration of KBr (0.99 mM) in this work would allow the primary particles to stay in close proximity and aggregate, thereby promoting the dominance of attachment-based growth while impeding the competitive atomic deposition. As confirmed by TEM images, cube-like aggregates composed of multiple Pd primary particles were formed as the intermediate at 100 °C, followed by their evolution into single-crystal cubes through fusion, recrystallization, and faceting (Figure 3). Another factor contributing to the formation of Pd cubes through an attachment process instead of atomic deposition is the ineffectiveness of PVP as a colloidal stabilizer in the current system. Although PVP was used at a concentration (74 mM) comparable to that in the conventional synthesis (86 mM) (Table S2), the initial reduction rate in the current system at 100 °C was significantly higher relative to that in the conventional synthesis due to the much lower concentration of KBr [200 times lower (Table S2)], resulting in an abundance of primary particles generated at the beginning of the synthesis. With a larger number of primary particles and thus more surface atoms that require coverage, the PVP would potentially be ineffective as a colloidal stabilizer to prevent the particles from aggregation, especially at a low concentration used in this work.

It should be pointed out that Br^- ions could also act as a regulator of the reduction kinetics, in addition to their common role in passivating the {100} facets of Pd

https://doi.org/10.1021/acs.chemmater.1c02791
Chem. Mater. 2021, 33, 8430–8439

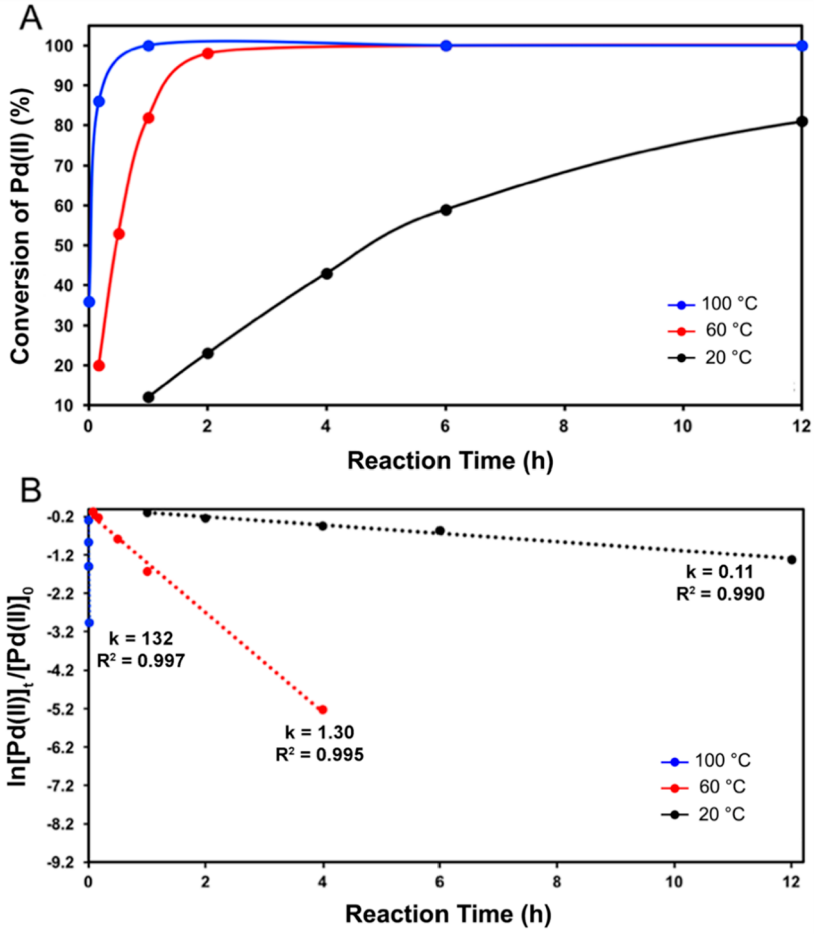

Figure 6. Plots showing (A) the percentage conversion of the Pd(II) precursor to Pd atoms through reduction by hydroquinone and (B) $\ln[Pd(II)]_t/[Pd(II)]_0$ as a function of reaction time at 100, 60, and 20 °C, as traced by blue, red, and black lines, respectively.

nanostructures. When dissolved in a solution containing $PdCl_4^{2-}$, Br^- ions could coordinate to the Pd(II) center through a ligand exchange process ($PdCl_4^{2-} + 4Br^- \rightarrow PdBr_4^{2-} + 4Cl^-$), generating $PdBr_4^{2-}$ as the new precursor and thus altering the reduction kinetics.[28] Because the standard reduction potential of $PdBr_4^{2-}$/Pd [0.49 V vs the reversible hydrogen electrode (RHE)] is more negative than that of $PdCl_4^{2-}$/Pd (0.62 V vs RHE), it is more difficult to reduce $PdBr_4^{2-}$ than $PdCl_4^{2-}$.[29] Consequently, if Br^- ions were used in great abundance, the reduction kinetics would be substantially slowed due to the dominance of $PdBr_4^{2-}$ species in the system. On the basis of this phenomenon, the slower initial reduction rate in the conventional synthesis relative to that in the current system at 100 °C could also originate from a much higher concentration of Br^- ions used for the synthesis (Table S2).

Influence of Temperature on Reduction Kinetics, Attachment, Surface Diffusion, and Fusion. To gain quantitative insight into the growth mechanism of different Pd nanostructures, we also measured the reduction kinetics of the Pd(II) precursor in the syntheses conducted at 20, 60, and 100 °C. As shown in Figure 6A, the reaction kinetics had a strong dependence on temperature. At 100 °C, the Pd(II) precursor was quickly depleted within the first hour, while only 80% conversion was achieved after 12 h at 20 °C. It is noteworthy that the two distinct trends in the conversion of the Pd(II) precursor to Pd atoms also validated the different growth pathways at 60 °C, including attachment of small primary particles and then atomic deposition to generating final products. The first trend extended from the start of the synthesis, displaying a sharp increase in conversion, followed by a gradual plateau at 1 h as a second trend that persisted for the rest of the synthesis. These two trends at 60 °C, equivalent to two different growth modes of Pd nanostructures, strongly indicate that the attachment process is dominant in the first hour of the synthesis while atomic deposition prevails in the remaining time. In contrast, for the reaction at 100 °C, the conversion of the Pd(II) precursor instantly reached a maximum in the first few minutes of a synthesis, suggesting that no additional growth through atomic deposition was possible after the complete depletion of the Pd(II) precursor from the solution. Instead, the fusion of Pd primary particles in each cube-like aggregate would be the main process directing the formation of final products. When $\ln[Pd(II)]_t/[Pd(II)]_0$ was plotted as a function of reaction time (Figure 6B), the linear dependence suggested that the reactions could be described by a first-order rate law. Remarkably, the calculated rate constants (k) at 100 and 60 °C were 1200 and 11.8 times greater, respectively, than that at 20 °C. When combined with the initial concentration of the Pd(II) precursor (0.99 mM), the corresponding initial reduction rate at 100 °C was found to be 1000-fold greater than that at 20 °C (Table S1). The significant difference in initial reduction rates further attested to the inverse correlation between the temperature and the

https://doi.org/10.1021/acs.chemmater.1c02791
Chem. Mater. 2021, 33, 8430−8439

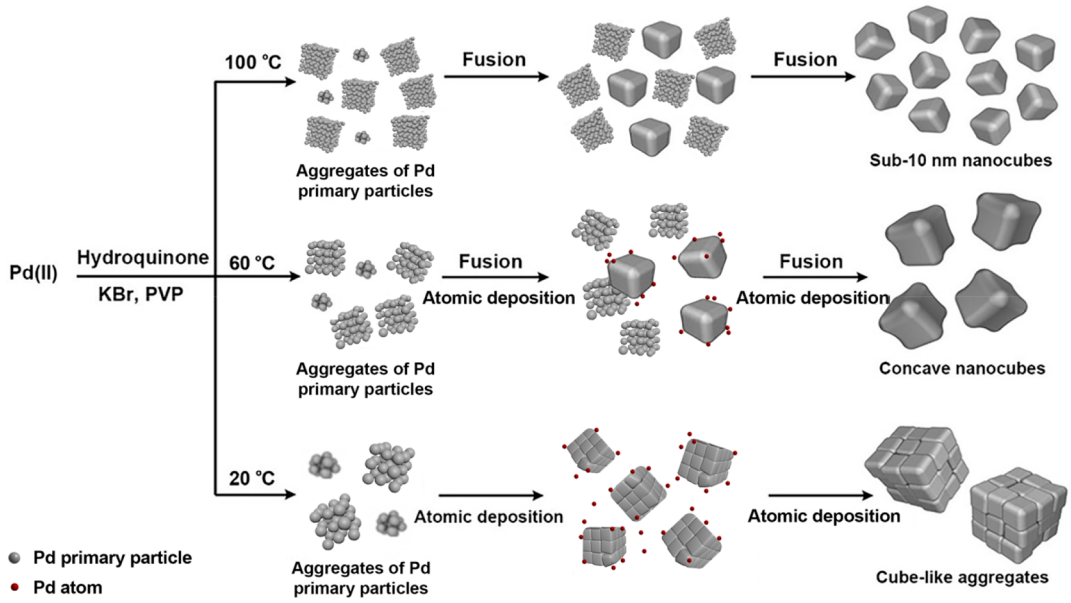

Figure 7. Growth mechanisms proposed to account for the formation of Pd nanocubes, concave cubes, and cube-like aggregates at different temperatures. In the presence of Br^- ions as a capping agent, the aggregates comprised of spatially separated primary particles formed in the early stage took a pseudocubic shape. The constituent particles in each aggregate then fused together to generate nanocubes at 100 °C. When the synthesis was conducted at 60 °C, the primary particles could still aggregate and fuse to form nanocubes, followed by atomic deposition at the corners and edges for the generation of concave nanocubes. When the reaction temperature was further decreased to 20 °C, fusion would be impeded by the substantially slow rate for surface diffusion. In this case, the primary particles in each aggregate could still grow through atomic deposition, giving rise to larger cube-like aggregates as final products.

sizes of primary particles and final products discussed in previous sections. Specifically, an increased initial reduction rate associated with an increased temperature would lead to the immediate formation of small primary particles in large amounts during the nucleation step. Together with a smaller amount of the precursor allocated, the extremely small building units would correspond to smaller products compared to those generated at room temperature.

In addition to the reaction kinetics, fusion of the primary particles and surface diffusion of atoms are two integral factors in controlling the shape evolution of metal nanostructures. In our study, despite the temperature changes, Pd primary particles are initially formed and then assembled into loose, cube-like aggregates in all reactions, serving as the precursor to the following growth of the nanostructures. However, the fusion rate varied significantly when shifting between reaction temperatures. Specifically, a considerably high temperature, such as 60 or 100 °C, would provide adequate kinetic energy for the primary particles in each aggregate to move in space and fuse together, followed by recrystallization with the assistance of a capping agent for the formation of single-crystal nanostructures with well-defined facets. When the temperature was too low, larger polycrystalline aggregates instead of single-crystal products would be generated because fusion was retarded by the slow motion of constituent particles and atoms. Moreover, it has been demonstrated that the final shape or morphology of the metal nanostructures was largely governed by the ratio of the atom deposition rate to the surface atom diffusion rate.[30] The transformation from concave to flat surfaces could be achieved if the deposition is relatively slow while the temperature is high enough to transport atoms to other sites through adequate surface diffusion rather than gathering at the corners. This concept was recently validated by an *in situ* TEM study on the growth trajectories of Pd@Pt core−shell nanocubes.[31]

Taken together, we propose a nonclassical growth mechanism to account for the generation of the various types of nanostructures at different temperatures, as illustrated in Figure 7. At the beginning of the synthesis, the Pd(II) precursor was reduced by hydroquinone to Pd atoms, which were supersaturated for the generation of Pd primary particles through homogeneous nucleation, whereas the initial reduction rate varied significantly with reaction temperature. As the reaction ensued, the primary particles with a high surface energy would easily aggregate through collision and attachment. With the aid of Br^- ions as a capping agent toward Pd{100} facets, the aggregates composed of spatially separated particles took a pseudocubic shape to promote the exposure of {100} facets on the surface. When the reaction proceeds at a high temperature of 100 °C, the Pd(II) precursor was quickly depleted within a very short period of time, terminating the growth of the initially formed aggregates due to the lack of atomic supply. Having an extremely small size as their merit, coupled with the kinetic energy endowed by increased temperature, the constituent particles and atoms in each aggregate could instead move faster in space and fuse together into a single-crystal nanostructure bearing a cubic shape and the inclusion of defects. This hypothesis is consistent with the observation in Figure 3D, where no aggregation was observed at 5 min into the synthesis, the turning point at which fusion would override the initial attachment. From a thermodynamic viewpoint, the elimination of defects via recrystallization and surface diffusion processes is highly favorable to achieve a minimum total surface energy in the nanoscale system. Therefore, the fast diffusion rate at 100 °C allowed the atoms to evenly spread across the surface of the particle under the capping effect of Br^- ions, initiating the reconstruction in

https://doi.org/10.1021/acs.chemmater.1c02791
Chem. Mater. 2021, 33, 8430−8439

structure and shape to smooth the surface of the nanocrystals. During this recrystallization process, Br^- ions promoted the formation of {100} facets by decreasing their surface energy, leading to the formation of sub-10 nm nanocubes enclosed by well-defined {100} facets as final products.

When the reaction temperature was decreased to 60 °C, the initial reduction took place at a slower rate, producing fewer primary particles that were relatively larger than those formed at 100 °C. The subsequent attachment of those primary particles to aggregates was also decelerated, leaving more particles and more Pd(II) precursor in the solution for the following steps. Supplied with newly formed Pd atoms and adequate energy at an intermediate temperature, the loose, cube-like aggregates could evolve into nanocubes with a minor degree of truncation via both fusion of the constituent particles and atomic deposition. In most cases, the constituent particles and atoms in each aggregate could directly fuse together to yield single-crystal, cubic nanostructures. As a secondary route, the individual particles situated at the uncapped sites (e.g., edges and corners) of each aggregate could first grow through atomic deposition and then undergo the fusion process once their sizes had reached a certain threshold. Regardless of whether fusion of the attached particles transpired directly or in tandem with atomic deposition, the first emergence of nanocubes derived from the loose, cube-like aggregates in the solution signaled the switch in growth mode to site-selective atomic deposition for the generation of concave nanocubes. During the final growth, the just-formed Pd atoms preferred to selectively deposit at the exposed corners and edges of the preformed nanocubes because the Pd{100} side faces were blocked by the chemisorbed Br^- ions. Because atom diffusion was substantially slower at 60 °C, most Pd atoms would accumulate at the corners and edges of the growing nanostructures due to the lack of time and kinetic energy for diffusion. As a result, larger concave nanocubes were finally obtained at 60 °C.

Following the proposed growth mechanism, it would be expected that the slowest initial reduction rate at 20 °C should result in the least number of primary particles with enlarged sizes relative to those formed at 60 and 100 °C. Under the influence of surface capping, loose, cube-like aggregates comprised of primary particles were still formed as intermediates through an attachment process, albeit over a much longer period of time. Because essentially no fusion could occur due to the inadequate kinetic energy at such a low temperature, more aggregates were available for the succeeding steps. Because these aggregates did not have single-crystal structures and well-defined {100} facets, their surfaces were inherently heterogeneous, with various sites not covered by Br^- ions, such as edges, corners, and spaces between the spatially separated constituent particles. With a significantly higher concentration of the Pd(II) precursor remaining in the reaction solution and thus more newly formed Pd atoms, atomic deposition took place on the primary particles located on the exposed sites of each aggregate. At the same time, a relatively small degree of surface diffusion could still occur at 20 °C, allowing some Pd atoms to be transported across the cavities in the structure of the aggregates. Thus, all constituent particles, including those inside the small aggregates, were able to grow through atomic deposition until all of the Pd(II) precursor had been completely consumed. Once the overgrowth stage ceased, these larger, pseudocubic aggregates would gradually evolve into a more cubic shape due to the diffusion of some atoms across the surface to promote shape focusing with the assistance of Br^- ions as a capping agent. Taken together, the varying reduction kinetics, attachment, fusion, and surface diffusion rates influenced by temperature collectively contributed to the generation of various types of cubic nanostructures at different temperatures.

CONCLUSIONS

In summary, we have demonstrated a new approach to produce different types of Pd cubic nanostructures, in which the Pd(II) precursor was reduced by hydroquinone at different temperatures, with Br^- ions serving as the capping agent. The generation of cubic nanostructures followed an attachment-based growth pathway instead of the commonly observed classical nucleation and growth of nanocrystals. In the synthesis, Pd primary particles were formed in the early stage and attached into cube-like aggregates under the capping effect from Br^- ions, which then served as seeds for the subsequent growth. As the reaction temperature was decreased from 100 to 20 °C, the final products would switch from sub-10 nm cubes to concave cubes and finally cube-like aggregates of much smaller particles. The varied morphologies of the cubic nanostructures obtained at different temperatures could be attributed to the combined effect from the changes in reduction kinetics, attachment, fusion of the primary particles, and surface diffusion of atoms induced by adequate kinetic energy. We believe that the mechanisms discovered herein provide an advanced understanding of the attachment-based growth behavior in colloidal synthesis of metal nanocrystals and can be extended to a broader range of inorganic materials.

ASSOCIATED CONTENT

Supporting Information

The Supporting Information is available free of charge at https://pubs.acs.org/doi/10.1021/acs.chemmater.1c02791.

TEM and STEM images of various Pd nanostructures obtained at three different temperatures (100, 60, and 20 °C); morphological evolution of the Pd nanostructures prepared at 60 °C in the absence of KBr; TEM images of various Pd nanostructures obtained at 60 and 100 °C when varying the volume of KBr added; and tables summarizing the results when the synthesis was conducted at three different temperatures and comparing the experimental parameters used in this work with those of the conventional protocol (PDF)

AUTHOR INFORMATION

Corresponding Author

Younan Xia − *The Wallace H. Coulter Department of Biomedical Engineering, Georgia Institute of Technology and Emory University, Atlanta, Georgia 30332, United States; School of Chemistry and Biochemistry, Georgia Institute of Technology, Atlanta, Georgia 30332, United States;* orcid.org/0000-0003-2431-7048; Email: younan.xia@bme.gatech.edu

Authors

Anderson G. M. da Silva − *The Wallace H. Coulter Department of Biomedical Engineering, Georgia Institute of Technology and Emory University, Atlanta, Georgia 30332, United States; Materials and Chemical Engineering*

Department, Pontifical Catholic University of Rio de Janeiro (PUC-Rio), 22453-900 Rio de Janeiro, RJ, Brazil

Ruhui Chen − *School of Chemistry and Biochemistry, Georgia Institute of Technology, Atlanta, Georgia 30332, United States*

Quynh N. Nguyen − *School of Chemistry and Biochemistry, Georgia Institute of Technology, Atlanta, Georgia 30332, United States;* orcid.org/0000-0003-1544-6139

Madeline Vara − *School of Chemistry and Biochemistry, Georgia Institute of Technology, Atlanta, Georgia 30332, United States*

Pedro H. C. Camargo − *Department of Chemistry, University of Helsinki, FI-00014 Helsinki, Finland;* orcid.org/0000-0002-7815-7919

Complete contact information is available at: https://pubs.acs.org/10.1021/acs.chemmater.1c02791

Notes

The authors declare no competing financial interest.

■ ACKNOWLEDGMENTS

This work was supported by the National Science Foundation (CHE-1804970) and startup funds from the Georgia Institute of Technology. A.G.M.d.S. thanks CNPq for a Science Without Borders fellowship. TEM imaging was performed at the Georgia Tech Institute for Electronics and Nanotechnology, a member of the National Nanotechnology Coordinated Infrastructure (NNCI), which is supported by the National Science Foundation (ECCS-2025462).

■ REFERENCES

(1) Xia, Y.; Xiong, Y.; Lim, B.; Skrabalak, S. E. Shape-Controlled Synthesis of Metal Nanocrystals: Simple Chemistry Meets Complex Physics? *Angew. Chem., Int. Ed.* **2009**, *48*, 60−103.

(2) Slater, T. J. A.; Macedo, A.; Schroeder, S. L. M.; Burke, M. G.; O'Brien, P.; Camargo, P. H. C.; Haigh, S. J. Correlating Catalytic Activity of Ag−Au Nanoparticles with 3D Compositional Variations. *Nano Lett.* **2014**, *14*, 1921−1926.

(3) da Silva, A. G. M.; Rodrigues, T. S.; Slater, T. J. A.; Lewis, E. A.; Alves, R. S.; Fajardo, H. V.; Balzer, R.; da Silva, A. H. M.; de Freitas, I. C.; Oliveira, D. C.; et al. Controlling Size, Morphology, and Surface Composition of AgAu Nanodendrites in 15 s for Improved Environmental Catalysis under Low Metal Loadings. *ACS Appl. Mater. Interfaces* **2015**, *7*, 25624−25632.

(4) Xie, S.; Choi, S.-I.; Xia, X.; Xia, Y. Catalysis on Faceted Noble-Metal Nanocrystals: Both Shape and Size Matter. *Curr. Opin. Chem. Eng.* **2013**, *2*, 142−150.

(5) Yuan, Q.; Wang, X. Aqueous-Based Route toward Noble Metal Nanocrystals: Morphology-Controlled Synthesis and Their Applications. *Nanoscale* **2010**, *2*, 2328−2335.

(6) Zhang, H.; Jin, M.; Xiong, Y.; Lim, B.; Xia, Y. Shape-Controlled Synthesis of Pd Nanocrystals and Their Catalytic Applications. *Acc. Chem. Res.* **2013**, *46*, 1783−1794.

(7) Mostafa, S.; Behafarid, F.; Croy, J. R.; Ono, L. K.; Li, L.; Yang, J. C.; Frenkel, A. I.; Cuenya, B. R. Shape-Dependent Catalytic Properties of Pt Nanoparticles. *J. Am. Chem. Soc.* **2010**, *132*, 15714−15719.

(8) Xu, R.; Wang, D.; Zhang, J.; Li, Y. Shape-Dependent Catalytic Activity of Silver Nanoparticles for the Oxidation of Styrene. *Chem. - Asian J.* **2006**, *1*, 888−893.

(9) Shi, Y.; Lyu, Z.; Zhao, M.; Chen, R.; Nguyen, Q. N.; Xia, Y. Noble-Metal Nanocrystals with Controlled Shapes for Catalytic and Electrocatalytic Applications. *Chem. Rev.* **2021**, *121*, 649−735.

(10) Jin, M.; Zhang, H.; Xie, Z.; Xia, Y. Palladium Nanocrystals Enclosed by {100} and {111} Facets in Controlled Proportions and Their Catalytic Activities for Formic Acid Oxidation. *Energy Environ. Sci.* **2012**, *5*, 6352−6357.

(11) Jin, M.; Zhang, H.; Xie, Z.; Xia, Y. Palladium Concave Nanocubes with High-Index Facets and Their Enhanced Catalytic Properties. *Angew. Chem., Int. Ed.* **2011**, *50*, 7850−7854.

(12) Xia, Y.; Xia, X.; Peng, H.-C. Shape-Controlled Synthesis of Colloidal Metal Nanocrystals: Thermodynamic versus Kinetic Products. *J. Am. Chem. Soc.* **2015**, *137*, 7947−7966.

(13) Yang, T.-H.; Peng, H.-C.; Zhou, S.; Lee, C.-T.; Bao, S.; Lee, Y.-H.; Wu, J.-M.; Xia, Y. Toward a Quantitative Understanding of the Reduction Pathways of a Salt Precursor in the Synthesis of Metal Nanocrystals. *Nano Lett.* **2017**, *17*, 334−340.

(14) Thanh, N. T. K.; Maclean, N.; Mahiddine, S. Mechanisms of Nucleation and Growth of Nanoparticles in Solution. *Chem. Rev.* **2014**, *114*, 7610−7630.

(15) Ashley, A. E.; Thompson, A. L.; O'Hare, D. Non-Metal-Mediated Homogeneous Hydrogenation of CO_2 to CH_3OH. *Angew. Chem., Int. Ed.* **2009**, *48*, 9839−9843.

(16) You, H.; Fang, J. Particle-Mediated Nucleation and Growth of Solution-Synthesized Metal Nanocrystals: A New Story beyond the LaMer Curve. *Nano Today* **2016**, *11*, 145−167.

(17) Ataee-Esfahani, H.; Skrabalak, S. E. Attachment-Based Growth: Building Architecturally Defined Metal Nanocolloids Particle by Particle. *RSC Adv.* **2015**, *5*, 47718−47727.

(18) Lv, W.; He, W.; Wang, X.; Niu, Y.; Cao, H.; Dickerson, J. H.; Wang, Z. Understanding the Oriented-Attachment Growth of Nanocrystals from an Energy Point of View: a Review. *Nanoscale* **2014**, *6*, 2531−2547.

(19) Wang, Y.; Choi, S.-I.; Zhao, X.; Xie, S.; Peng, H.-C.; Chi, M.; Huang, C. Z.; Xia, Y. Polyol Synthesis of Ultrathin Pd Nanowires via Attachment-Based Growth and Their Enhanced Activity towards Formic Acid Oxidation. *Adv. Funct. Mater.* **2014**, *24*, 131−139.

(20) Cao, Y.; Yang, Y.; Shan, Y.; Fu, C.; Viet Long, N.; Huang, Z.; Guo, X.; Nogami, M. Large-Scale Template-Free Synthesis of Ordered Mesoporous Platinum Nanocubes and Their Electrocatalytic Properties. *Nanoscale* **2015**, *7*, 19461−19467.

(21) Wang, Y.; Zheng, Y.; Huang, C. Z.; Xia, Y. Synthesis of Ag Nanocubes 18−32 nm in Edge Length: The Effects of Polyol on Reduction Kinetics, Size Control, and Reproducibility. *J. Am. Chem. Soc.* **2013**, *135*, 1941−1951.

(22) Xie, S.; Choi, S.-I.; Lu, N.; Roling, L. T.; Herron, J. A.; Zhang, L.; Park, J.; Wang, J.; Kim, M. J.; Xie, Z.; et al. Atomic Layer-by-Layer Deposition of Pt on Pd Nanocubes for Catalysts with Enhanced Activity and Durability toward Oxygen Reduction. *Nano Lett.* **2014**, *14*, 3570−3576.

(23) Xiong, Y.; Cai, H.; Wiley, B. J.; Wang, J.; Kim, M. J.; Xia, Y. Synthesis and Mechanistic Study of Palladium Nanobars and Nanorods. *J. Am. Chem. Soc.* **2007**, *129*, 3665−3675.

(24) Lim, B.; Jiang, M.; Tao, J.; Camargo, P. H. C.; Zhu, Y.; Xia, Y. Shape-Controlled Synthesis of Pd Nanocrystals in Aqueous Solutions. *Adv. Funct. Mater.* **2009**, *19*, 189−200.

(25) Jehannin, M.; Rao, A.; Cölfen, H. New Horizons of Nonclassical Crystallization. *J. Am. Chem. Soc.* **2019**, *141*, 10120−10136.

(26) Xue, X.; Penn, R. L.; Leite, E. R.; Huang, F.; Lin, Z. Crystal Growth by Oriented Attachment: Kinetic Models and Control Factors. *CrystEngComm* **2014**, *16*, 1419−1429.

(27) Jin, M.; Liu, H.; Zhang, H.; Xie, Z.; Liu, J.; Xia, Y. Synthesis of Pd Nanocrystals Enclosed by {100} Facets and with Sizes < 10 nm for Application in CO Oxidation. *Nano Res.* **2011**, *4*, 83−91.

(28) Zhou, M.; Wang, H.; Vara, M.; Hood, Z. D.; Luo, M.; Yang, T. H.; Bao, S.; Chi, M.; Xiao, P.; Zhang, Y.; Xia, Y. Quantitative Analysis of the Reduction Kinetics Responsible for the One-Pot Synthesis of Pd-Pt Bimetallic Nanocrystals with Different Structures. *J. Am. Chem. Soc.* **2016**, *138*, 12263−12270.

(29) Xie, M.; Zhou, S.; Zhu, J.; Lyu, Z.; Chen, R.; Xia, Y. A Quantitative Analysis of the Reduction Kinetics Involved in the Synthesis of Au@Pd Concave Nanocubes. *Chem. - Eur. J.* **2019**, *25*, 16397−16404.

(30) Xia, X.; Xie, S.; Liu, M.; Peng, H.-C.; Lu, N.; Wang, J.; Kim, M. J.; Xia, Y. On the Role of Surface Diffusion in Determining the Shape or Morphology of Noble-Metal Nanocrystals. *Proc. Natl. Acad. Sci. U. S. A.* **2013**, *110*, 6669−6673.
(31) Gao, W.; Elnabawy, A. O.; Hood, Z. D.; Shi, Y.; Wang, X.; Roling, L. T.; Pan, X.; Mavrikakis, M.; Xia, Y.; Chi, M. Atomistic Insights into the Nucleation and Growth of Platinum on Palladium Nanocrystals. *Nat. Commun.* **2021**, *12*, 3215.

https://doi.org/10.1021/acs.chemmater.1c02791
Chem. Mater. 2021, 33, 8430−8439